Title

Nicotinamide riboside activates renal metabolism and protects the kidney in a model of Alport syndrome

Authors

Bryce A. Jones,[1] Debora L. Gisch,[2] Komuraiah Myakala,[3] Amber Sadiq,[3] Ying-Hua Cheng,[2] Elizaveta Taranenko,[4,5] Julia Panov,[5] Kyle Korolowicz,[6] Xiaoxin Wang,[3] Avi Z. Rosenberg,[7] Sanjay Jain,[8] Michael T. Eadon,[2] Moshe Levi[3]

Affiliations

[1]Department of Pharmacology and Physiology, Georgetown University, Washington, DC, USA

[2]Department of Medicine, Division of Nephrology, Indiana University School of Medicine, Indianapolis, IN, USA

[3]Department of Biochemistry and Molecular & Cellular Biology, Georgetown University, Washington, DC, USA

[4]Department of Biology, University of La Verne, La Verne, CA, USA

[5]Tauber Bioinformatics Research Center, University of Haifa, Haifa, Israel

[6]Department of Microbiology and Immunology, Georgetown University, Washington, DC, USA

[7]Department of Pathology, Johns Hopkins University School of Medicine, Baltimore, MD, USA

[8]Department of Medicine, Washington University School of Medicine, St. Louis, MO, USA

Corresponding Author

Moshe Levi

Basic Science Building, Room 353

3900 Reservoir Rd NW

Washington, DC 20007

ORCiD

Bryce A. Jones (0000-0002-6950-8414)

Debora L. Gisch (0000-0001-9087-4585)

Komuraiah Myakala (0000-0003-3233-047X, 0000-0001-5105-1252)

Amber Sadiq (0009-0002-9394-7510)

Elizaveta Taranenko (0009-0009-1680-5202)

Julia Panov (0000-0003-2392-4073)

Kyle Korolowicz (0000-0003-1116-6500)

Xiaoxin Wang (0000-0001-9205-6228)

Avi Z. Rosenberg (0000-0003-2356-950X)

Sanjay Jain (0000-0003-2804-127X)

Michael T. Eadon (0000-0003-3066-2876)

Moshe Levi (0000-0002-6225-946X, 0000-0001-6403-2261)

Abstract

Chronic kidney disease (CKD) is associated with renal metabolic disturbances, including impaired fatty acid oxidation (FAO). Nicotinamide adenine dinucleotide (NAD^+) is a small molecule that participates in hundreds of metabolism-related reactions. NAD^+ levels are decreased in CKD, and NAD^+ supplementation is protective. However, both the mechanism of how NAD^+ supplementation protects from CKD, as well as the cell types most responsible, are poorly understood. Using a mouse model of Alport syndrome, we show that nicotinamide riboside (NR), an NAD^+ precursor, stimulates renal peroxisome proliferator-activated receptor α signaling and restores FAO in the proximal tubules, thereby protecting from CKD in both sexes. Bulk RNA-sequencing shows that renal metabolic pathways are impaired in Alport mice and dramatically activated by NR in both sexes. These transcriptional changes are confirmed by orthogonal imaging techniques and biochemical assays. Single nuclei RNA-sequencing and spatial transcriptomics, both the first of their kind from Alport mice, show that NAD^+ supplementation restores FAO in the proximal tubules with minimal effects on the podocytes. Finally, we also report, for the first time, sex differences at the transcriptional level in this Alport model. Male Alport mice had more severe inflammation and fibrosis than female mice at the transcriptional level. In summary, the data herein identify both the protective mechanism and location of NAD^+ supplementation in this model of CKD.

Introduction

Chronic kidney disease (CKD) is a clinical diagnosis characterized by the gradual loss of renal function, and it is a substantial cause of morbidity and mortality. The pathophysiology of CKD is complex, and kidney diseases of distinct etiologies can all converge on CKD (1). Nevertheless, several unifying mechanisms emerge when comparing healthy kidneys to their diseased counterparts. These include the progressive worsening of renal fibrosis, inflammation, and metabolic disturbances. From this, it stands to reason that treatments that prevent these changes may also prevent the associated loss of renal function. Herein, we focus on preventing the progression of kidney disease by activating renal metabolism with the nicotinamide adenine dinucleotide (NAD^+) precursor, nicotinamide riboside (NR).

NAD^+ is essential to a wide range of metabolic reactions. As a coenzyme, it shuttles electrons through redox reactions by cycling between its oxidized (NAD^+) and reduced (NADH) states. As an essential cofactor, it post-translationally modifies proteins to regulate both the protein signaling pathways themselves and the gene regulatory networks they control. Given its central role, reduced NAD^+ levels should be expected to cause significant aberrations in metabolism (2).

It is well established that reduced NAD^+ levels contribute to acute kidney injury (AKI). During AKI, there is a simultaneous increase in NAD^+ consumption and a decrease NAD^+ synthesis (3). This causes a reduction in kidney NAD^+ levels and subsequent impairments in renal metabolism, including mitochondrial function, the citric acid cycle, and FAO (3, 4). NAD^+ supplementation has been shown to reverse these pathologies and to protect the kidney in multiple models of AKI, reviewed elsewhere (5). Mechanistic studies on NAD^+ supplementation

in models of AKI have been enlightening. Using both gain- and loss-of-function transgenic mice, Tran et al. (6) comprehensively showed that the peroxisome proliferator-activated receptor-γ coactivator 1-α (PGC-1α) protects from AKI by upregulating genes in the *de novo* NAD^+ synthesis pathway. PGC-1α is a coactivator that controls metabolism-related gene regulatory networks, including by direct interaction with the peroxisome proliferator-activated receptor α (PPARα) (7). Tran et al. (6) also observed a corresponding decrease in renal lipid accumulation and an increase in β-hydroxybutyrate, a key metabolite of fatty acid oxidation (FAO) with an additional role in cell signaling. These changes were replicated upon exogenous administration of nicotinamide. Their data clearly indicate that improvements in mitochondrial function, including FAO, substantially contribute to the protective effects of NAD^+ supplementation in AKI.

Studies are emerging that suggest reduced NAD^+ may also play a role in CKD. Endogenous NAD^+ biosynthesis is impaired in CKD, and there is a corresponding decrease in levels of NAD^+ and its related metabolites (8, 9). Although one study did not demonstrate a benefit (9), NAD^+ supplementation with nicotinamide, nicotinamide mononucleotide, and NR has generally been shown to protect against CKD (10-14). Preventing NAD^+ breakdown has also been shown to be protective (15). However, unlike in AKI, the mechanism of how NAD^+ protects the kidney in CKD is still poorly understood. A key limitation is that no study thus far has investigated the cell type specific effects of NAD^+ supplementation in a model of CKD, and there exist conflicting data on if NAD^+ supplementation primarily affects the podocytes or the renal tubules (10-12).

Recent data from our lab suggested that NAD^+ supplementation may modulate expression of metabolic genes in a model of diabetic CKD, although it was not the main focus of the study (14). In that study, we demonstrated that NR treatment restored mitochondrial function via sirtuin 3 activation, thereby preventing mitochondrial damage and subsequent leak of mitochondrial DNA into the cytosol. This reduced activation of the cyclic GMP–AMP synthase–stimulator of interferon genes pathway and thus protected the kidney. Importantly, we also identified changes in key genes involved in metabolism, including NR-mediated increases in kidney mRNA transcripts for *Ppargc1a*, *Nrf1*, *Tfam*, *Cpt1a*, *Acadm*, and *Acadl*. Because these genes are encoded in the nuclear genome, we found it unlikely that the changes were a direct result of mitochondrial sirtuin 3 activation. Instead, it implied a mechanism of NAD^+ supplementation that acted at the transcriptional level to modulate expression of key metabolic genes. We therefore sought to identify the molecular mechanism underlying this change.

To begin to dissect this mechanism, as well as cell types responsible, we returned to the NAD^+ supplementation data reported from models of AKI. We found the data reported by Tran et al. (6) to be very compelling evidence for the role of PGC-1α, and it was consistent with the transcriptional activation of metabolic genes that we observed in our recent study using a model of diabetic CKD (14). Furthermore, mitochondrial dysfunction and associated FAO defects are key metabolic disturbances that drive CKD (16, 17), and restoring renal metabolism has been shown to be protective (18). We therefore hypothesized that, similar to in AKI, NAD^+ supplementation would protect from CKD via PGC-1α–mediated activation of renal metabolism.

We next tested the hypothesis that if the mechanism of NAD^+ supplementation was indeed by restoring mitochondrial function and FAO, then it would have the greatest benefit on the cells most affected by impaired mitochondrial function and FAO. The proximal tubules contain some of the most metabolically active cells in the body, and their preferred energy substrate is fatty acids (16). In contrast to this, podocytes maintain the GBM by anerobic glycolysis (19). We therefore hypothesized that NAD^+ supplementation would be of substantial benefit to the proximal tubules with minimal effects on the podocytes.

To summarize the above information: 1) restoring NAD^+ protects from AKI via PGC-1α, 2) restoring NAD^+ in CKD is protective, 3) restoring renal metabolism in CKD is protective, but 4) the mechanism of how NAD^+ supplementation activates renal metabolism in CKD, as well as the cell types that are most affected in models of CKD, are largely unknown.

Given the above rationale, we hypothesized that NAD^+ supplementation with NR protects the kidney by activating renal metabolism in the proximal tubules, a highly metabolically active segment of the nephron. We tested this hypothesis with a three-step sequential approach. We first tested NR in a mouse model of Alport syndrome to show that NAD^+ supplementation protects against CKD. We then employed biochemical techniques, including RNA-sequencing (RNA-seq) and immunoblotting, to assess metabolic dysregulation. Finally, we performed single-nuclei RNA-seq (snRNA-seq) to show that NAD^+ supplementation specifically enhances renal metabolism in the proximal tubules, with minimal effects on the podocytes. The results presented herein provide strong evidence that NR activates the NAD^+–PGC-1α–PPARα–FAO axis in the proximal tubules, thereby stimulating metabolism and protecting the kidney.

Materials and Methods

Animal models

Animal studies were approved by the Institutional Animal Care and Use Committee of Georgetown University. *Col4a3*^{tm1Dec} mice on the C57BL/6J background slowly develop kidney disease, and they were obtained as a gift from Sanofi (Framingham, MA) (20, 21). Col4a3$^{-/-}$ was the disease genotype, and Col4a3$^{+/-}$ was the control genotype. Genotyping was performed by Transnetyx (Cordova, TN) using RT-qPCR. All experiments were conducted in male and female mice until we established a solid rationale for only studying a single sex.

For all studies, mice were housed at ambient temperature with a 12:12-hr light-dark cycle and free access to food and water. Litter-to-litter variation was controlled for by balancing treatment groups across litters. Nicotinamide riboside (CAS No. 1341-23-7) was obtained from ChromaDex (Los Angeles, CA) through participation in their External Research Program. Heparinized plasma and organs were collected upon euthanasia with carbon dioxide.

NAD^+ quantification in control and Alport mice

Control and Alport mice were maintained on a grain-based chow (Cat. No. 3005740-220, LabDiet, St. Louis, MO) and euthanized at 25 weeks old.

NAD^+ supplementation experiment in control and Alport mice

Control and Alport mice were maintained on a grain-based chow (Cat. No. 3005740-220, LabDiet) until 10 weeks old. They were then switched to a purified control diet alone (Cat. No. TD.130352, Envigo, Indianapolis, IN) or admixed with NR (0.5% w/w, Cat. No. TD.190868, Envigo) for the remainder of the study. Administration of this dose of NR to mice via the diet

has been reported previously (14). Photoplethysmography, echocardiography, and 24-hr urine collection were performed at 24-25 weeks old. Mice were euthanized at 25 weeks old.

Replication of NAD^+ supplementation experiment in Alport mice

Control and Alport mice were maintained on a grain-based chow (Cat. No. 3005740-220, LabDiet). NR was administered in the drinking water (5 g/L) to one half of the mice, starting at six-weeks of age. NR water was replaced twice per week. NR is stable in water dispensers for at least six days, and it does not affect water intake (22). Twenty-four–hour urine collection was performed at 24-25 weeks old, and mice were euthanized at 25 weeks old.

In vivo measurements

Urine was collected from mice by housing them in metabolic cages. Mice were habituated to the cages for one day prior to urine collection. Echocardiography (Vevo 3100, VisualSonics, Toronto, Canada) was performed by an experienced preclinical ultrasound technician as previously described (23) and in accordance with recent guidelines (24). Blood pressure was measured by tail photoplethysmography (Model BP-2000-M-6, Visitech Systems, Apex, NC). Habituation cycles were performed for the two days prior to collection of the blood pressure data.

Biochemical assays

NAD^+ was quantified in a mid-transverse kidney piece (Cat. No. E2ND-100, BioAssay Systems). Urine albumin (Cat. No. 1011, Ethos Biosciences, Logan Township, NJ) was determined according to the manufacturers' instructions. Expression of proteins of interest were quantified from a mid-transverse kidney piece by immunoblotting and normalized to total protein using Ponceau S as previously described (25). The primary antibodies used for

immunoblotting were CPT1α (Abcam, Cambridge, United Kingdom), fibronectin (Cat. No. F3648, MilliporeSigma, Burlington, MA), MCAD (Santa Cruz Biotechnology, Dallas, TX), and PGC-1α (Cat. No. AB3242, MilliporeSigma). The secondary antibodies were anti-rabbit (MilliporeSigma) and light chain-specific anti-mouse (Cat. No. AP200P, MilliporeSigma).

Histopathology and immunohistochemistry

Tissues were drop-fixed in 10% neutral buffered formalin for 24-hours at 4 ºC, dehydrated with an ethanol-xylene gradient, and embedded in paraffin. Formalin-fixed, paraffin-embedded tissues were sectioned (3 µm) onto glass slides using a microtome. Picrosirius red (PSR) staining was performed (Cat. No. SO-674, Rowley Biochemical, Danvers, MA), and polarized images were acquired with an IX83 Inverted Microscope (Olympus Scientific Solutions, Tokyo, Japan). PSR images were analyzed by thresholding in ImageJ2, and data are presented as the percent of pixels that stained positive (26). Immunohistochemistry for $p57^{kip2}$ (Cat. No. ab75975, Abcam) followed by periodic acid–Schiff (Cat. No. 22-110-645, Fisher Scientific, Hampton, NH) post-staining without hematoxylin counterstaining was performed and analyzed as previously described (27). Brightfield images were acquired with an Aperio GT 450 (Leica Microsystems, Wetzlar, Germany).

Analysis of previously published RNA-sequencing datasets

RNA-seq data from previously published RNA-seq experiments were downloaded from the Sequence Read Archive (SRA) (28). Accession numbers SRR1611815, SRR1611816, SRR1611817, SRR1611818, SRR1611819, SRR1611820, and SRR1611821 correspond to 3 male control and 4 male Alport kidneys, respectively, on the 129X1/SvJ background, 5.5 weeks of age (29). Accession numbers SRR15102716, SRR15102717, SRR15102718, SRR15102719,

SRR15102720, SRR15102721, SRR15102722, SRR15102723, SRR15102724, SRR15102725, and SRR15102726 correspond to 5 male control and 6 male Alport kidneys, respectively, on a mixed 129/SvJ and C57BL/6J background, 15 weeks of age (30). Sequencing files were aligned and processed with BioJupies, a webserver that automatically analyzes RNA-seq datasets and generates Jupyter Notebooks (31). Gene ontology (GO) enrichment analyses and Kyoto Encyclopedia of Genes and Genomes (KEGG) pathway analyses obtained from BioJupies were plotted in GraphPad Prism (San Diego, CA) (32-35).

Bulk RNA-sequencing and data analyses

Bulk RNA-seq was performed on isolated kidney cortex from 25-week-old *Col4a3*^{tm1Dec} mice on the C57BL/6J background. All eight combinations of experimental groups were investigated: male versus female, control versus Alport, and vehicle versus NR (N = 4 mice per group, 32 mice total). Total RNA was extracted with spin columns (Cat. No. 74104, Qiagen, Germantown, MD), and RNA-seq using the poly(A) selection method was performed by Genewiz (South Plainfield, NJ). Sequencing files were aligned, processes, and analyzed with BioJupies (31). GO enrichment analyses, KEGG pathway analyses, and transcription factor enrichment analyses were downloaded from BioJupies and further processed to identify statistically significant changes occurring in *a priori* defined comparisons, as described in the Results.

A separate analysis was performed to investigate a potential sex-genotype interaction. The subset of 16 vehicle-treated mice, 4 from each sex/genotype combination, were compared in a two-by-two factorial design using iDEP, a web application for analyzing previously aligned RNA-seq data (36). Differential gene expression between the sexes, the genotypes, and the

interaction term were calculated. Genes with both at least a two-fold change in expression and an adjusted *P*-value (FDR) less than 0.05 were deemed statistically significant.

All principal component analyses were performed using iDEP and plotted with GraphPad Prism (36). KEGG graphs were rendered by Pathview Web (37, 38).

Single nuclei RNA-sequencing

Single nuclei RNA-seq and the simultaneous assay for transposase-accessible chromatin were performed on kidneys from 25-week-old *Col4a3*^{tm1Dec} mice on the C57BL/6J background. All eight combinations of experimental groups were investigated: male vs. female, control vs. Alport, and vehicle vs. nicotinamide riboside (*N* = 1 mouse per group, 8 mice total). Male and female nuclei of the same genotype/treatment combination were pooled, and only the pooled snRNA-seq data are presented here.

For snRNA-seq, 49,488 nuclei were isolated from tissue cryosections and processed using the Chromium Next GEM Single Cell Multiome ATAC + Gene Expression (v1.0) kit as previously described (39). The RNA and ATAC libraries were sequenced separately on an Illumina NovaSeq 6000 system (Software v.1.7.0 and v.1.7.5). For RNA analysis, cell barcodes passing the following quality control filters were used for downstream analyses: 1) passed 10X Cell Ranger Arc (RNA) filters; 2) nCount_RNA showing greater than 1,000 and less than 25,000 in non-mitochondrial genes detected; and 3) cells with percentage of mitochondrial transcripts greater than 25 percent were removed. RNA counts were normalized using sctransform, and the clustering was done with 0.5 resolution. This integration was performed using Seurat (v.5.0.0). Cluster annotations are based on published gene markers (40) and converted by BioMart (v.2.56.1) to the mouse homologous genes. The differential expressed genes are

performed by RunPresto with logFC threshold = 0, Wilcox test, and corrected by Bonferroni from package SeuratWrappers (v.0.3.2). The pathway analyses were performed by pathfindR (v.2.3.0.9001) (41). The mmu_STRING database to identify relevant networks of protein interactions and mmu_KEGG database to contextualize these networks within known biological pathways are enriched.

Spatial transcriptomics

Spatial transcriptomics was performed on kidneys from 25-week-old *Col4a3*^{tm1Dec} mice on the C57BL/6J background. All four combinations of male experimental groups were investigated: control versus Alport, and vehicle versus NR (*N* = 1 male mouse per group, 4 mice total). The same tissue blocks were used for both snRNA-seq and spatial transcriptomics.

Murine kidney tissues were embedded in O.C.T. compound (Cat. No. 23-730-571, Fisher Scientific) immediately after euthanasia. Samples were processed according to the Visium Spatial Gene Expression protocol (10x Genomics, CG000240 protocol) (42). One sample from each condition underwent cryosectioning to yield a section of 10 µm thickness. The sections were stained with hematoxylin and eosin and imaged using a Keyence BZ-X810 microscope, equipped with a Nikon 10X CFI Plan Fluor objective lens. The brightfield images were compiled and matched with Visium fiducials to create comprehensive mosaics. The mRNA from the tissue sections was extracted following a 12-minute permeabilization period. This mRNA then adhered to oligonucleotides at the fiducial spots and was subsequently reverse transcribed. In the subsequent stages of library creation and sequencing, the mRNA was converted into second-strand cDNA. This was followed by denaturation, amplification of the cDNA, and purification using SPRIselect cDNA cleanup (Visium CG000239 protocol). Finally, the cDNA sequencing was

performed using an Illumina NovaSeq 6000 system. For spatial analysis, Space Ranger (v2.0.0) with the reference mouse genome (mm10-2020-A) was used to perform expression analysis, mapping, counting, and clustering. Labels were transferred from snRNA-seq to ST to spatially localize the cell types based on gene expression profiles using Seurat (v.5.0.0) onto 8,748 spots.

Statistical analyses for kits, immunoblots, and microscopy

One-way analysis of variance (ANOVA) was performed with GraphPad Prism. For ANOVA post-hoc tests, the decision to compare only the following groups was made *a priori*: (1) control + vehicle vs. control + NR, (2) control + vehicle vs. Alport + vehicle, (3) Alport + vehicle vs. Alport + NR, and (4) control + vehicle vs. Alport + NR.

Results

Alport mice have reduced NAD^+ levels and impaired renal metabolism

The first set of data we generated focused on validating our rationale for the study. To confirm that pathways related to both NAD^+ and renal metabolism are dysregulated in Alport mice, we re-analyzed previously published RNA-seq data from two independent experiments (29, 30). GO enrichment and KEGG pathway analyses were performed on the 500 most down-regulated genes in Alport mice, and both NAD^+ biosynthetic pathways (**Figs. S1A-B**) and fatty acid metabolic pathways (**Fig. S2**) were significantly enriched. This is in stark contrast to the pathways identified from analyses of up-regulated genes, most of which were related to inflammation and fibrosis (**Figs. S1C-D**) (25). Finally, we confirmed that kidney NAD^+ levels were lower in male and female Alport mice compared to control mice (**Figs. 1A-B**).

NAD^+ supplementation protects Alport mice from kidney disease

Given that kidney NAD^+ levels were decreased in Alport mice compared to control mice, we hypothesized that NAD^+ supplementation with NR would reduce the severity of kidney disease. To test this, control and Alport mice on the C57BL/6J background were treated with or without NR between the 10 and 25 weeks of age (**Fig. 2A**). We did not observe any changes in echocardiography or blood pressure measurements between the groups, excluding these as potential confounding variables (**Tables S1-2**). Twenty-four–hour urinary albumin excretion, a marker of kidney damage, was greatly increased in Alport mice, and NR treatment partially prevented this increase in both sexes (**Fig. 2B**). As shown by polarized microscopy of PSR-stained kidney sections, a technique that is highly specific for collagen (43), NR treatment prevented the progression of renal fibrosis in both sexes (**Figs. 2C-D**). The prevention of renal

fibrosis was secondarily confirmed by immunoblotting for fibronectin which was reduced in NR-treated male (significant, $P < .001$) and female (trend, $P < .10$) Alport mice (**Fig. S3**). We then repeated the experiment in both male and female mice, and the results were the same (**Fig. S4A**). Twenty-four–hour urinary albumin excretion was greatly increased in Alport mice, and NR treatment ameliorated this increase in both sexes (**Fig. S4B**). Both our initial and replication experiments had substantial numbers of littermate-matched mice in each group, and they were temporally separated by greater than one year.

NAD^+ supplementation treatment protects from glomerular and tubular injury in Alport mice

Glomerular damage was further assessed by immunostaining for the podocyte marker $p57^{kip2}$. Compared to control mice, Alport mice had reduced glomerular volumetric podocyte density, and NR treatment prevented this decline in both sexes (**Fig. 3A-B**). These results, in combination with the reduction in urinary albumin excretion, demonstrate that NR treatment protects from glomerular damage in the Alport model of kidney disease.

Although Alport syndrome is classically associated with a specific glomerular defect, there is strong data showing that glomerular injury can also cause tubular injury (44, 45). In addition, the proximal tubules are highly metabolically active, and they may have limited metabolic reserve to cope with increased protein leakage. This would be further exacerbated by an NAD^+ deficiency. We therefore hypothesized that Alport mice would exhibit substantial tubular pathology that was reversed by NR treatment. Consistent with our hypothesis, renal kidney injury molecule 1 (KIM-1) expression, a marker of tubular damage (46, 47), was increased in Alport mice, and NR treatment prevented this increase in both sexes (**Fig. 3C-F**). We then investigated the mechanism underlying this protective effect.

Bulk RNA-sequencing identifies renal cortical metabolic defects in Alport mice that are prevented by NAD^+ supplementation

We performed bulk RNA-seq on isolated kidney cortex to both confirm our hypothesis that NAD^+ supplementation normalizes renal metabolism and to identify if PGC-1α–PPARα signaling is the molecular mechanism driving this change. Principal component analysis demonstrated separation by genotype (PC1, 42.7% of variance, $P = 2.75\times10^{-11}$), sex (PC2, 11.3% of variance, $P = 1.16\times10^{-07}$), and treatment (PC3, 7.3% of variance, $P = 2.07\times10^{-03}$). In both sexes, NR treatment shifted Alport samples towards the control genotype, suggesting the prevention of the disease process (**Fig. S5**).

For each sex, we then performed GO enrichment and KEGG pathway analyses comparing: 1) NR-treated control mice vs. vehicle-treated control mice; 2) vehicle-treated Alport mice vs. vehicle-treated control mice; and 3) NR-treated Alport mice vs. vehicle-treated Alport mice. The decision to compare these groups was made *a priori* as they are the most relevant biological comparisons.

Consistent with our hypothesis, GO enrichment analyses revealed that numerous metabolism-related biological processes were changed between the groups. In both sexes, GO biological processes involving fatty acids, including fatty acid β-oxidation, were among the most highly enriched set of processes that were simultaneously downregulated in vehicle-treated Alport mice (versus vehicle-treated control mice) (**Figs. 4A** and **S6A**) and upregulated in NR-treated Alport mice (versus vehicle-treated Alport mice) (**Figs. 4B** and **S6B**). Many GO biological processes that are integral to energy metabolism were also simultaneously enriched in both comparisons, including acetyl-CoA metabolic process and acyl-CoA metabolic process (**Figs. 4A-**

B and **S6A-B**). KEGG pathway analyses yielded similar results in both sexes (**Figs. 4C-D** and **S6C-D**). The severe impairment of renal metabolism in Alport mice is evident by the downregulation of genes involved in metabolic pathways (KEGG Entry No. 01100) with an adjusted *P*-value (FDR) approaching forty orders of magnitude in both sexes (**Figs. 4C** and **S6C**). Transcription factor analyses revealed differential activity of the RXR/PPARα heterodimer as a likely candidate underlying the observed transcriptional differences (**Figs. 4E-F** and **S6E-F**).

Based on the data from the GO enrichment, KEGG pathway, and transcription factor analyses, we plotted the gene changes on KEGG graphs for the PPAR signaling pathway (KEGG Entry No. 03320) (**Figs. 4G**, **S6G**, and **S7-8**), the peroxisome (KEGG Entry No. 04146) (**Figs. S9-10**), and fatty acid degradation (KEGG Entry No. 00071) (**Figs. S11-12**). A multitude of genes involved in these pathways, especially those related to FAO, were reduced in vehicle-treated Alport mice (compared to vehicle-treated control mice) and restored in NR-treated Alport mice (compared to vehicle-treated Alport mice). Data from both comparisons are visualized simultaneously on the KEGG graphs, the former on the left half of each rectangle, and the latter on the right half.

All together, these data represent clear evidence for impaired renal metabolism in Alport mice, including fatty acid metabolism, that is restored by NR treatment. Next, we investigated NR treatment in control mice to confirm that NR is directly responsible for normalizing renal metabolism.

NAD^+ supplementation activates renal metabolism in control mice, confirming this as the causal mechanism of NR-mediated kidney protection

Although the dramatic change in metabolic state between vehicle- and NR-treated Alport mice suggests that NR protects the kidney by activating renal metabolism, it is not enough alone to show a causal relationship. In other words, because renal metabolism in Alport mice becomes gradually more impaired as kidney disease progresses, any intervention that reduces kidney disease will also cause a coincidental improvement of renal metabolism. This is not because the intervention activates renal metabolism, *per se*. It is instead an artifact that arises because the intervention-treated group has less severe kidney disease than the vehicle-treated group at the timepoint of study. To truly determine the mechanism of a drug, it is necessary to investigate its effects in healthy control mice. We therefore compared NR-treatment to vehicle-treatment in control mice, and we juxtapose this with the comparison of NR-treatment to vehicle-treatment in Alport mice.

In both sexes, metabolism-related GO biological processes were among the most highly enriched set that were simultaneously upregulated in both NR-treated control mice (versus vehicle-treated control mice) (**Figs. S13A** and **S14A**) and in NR-treated Alport mice (versus vehicle-treated Alport mice) (**Figs. S13B** and **S14B**). KEGG pathway analyses mirrored these results (**Figs. S13C** and **S14C**), and transcription factor analyses also predicted the activation of RXR/PPARα in the NR-treated samples (**Figs. S13D** and **S14D**). The striking similarity of NR treatment in both control and Alport mice is demonstrated by visualization on KEGG graphs for the PPAR signaling pathway (KEGG Entry No. 03320) (**Figs. S15-16**), the peroxisome (KEGG Entry No. 04146) (**Figs. S17-18**), and fatty acid degradation (KEGG Entry No. 00071) (**Figs. S19-20**).

In summary, the effect of NR treatment on metabolism-related pathways in control mice was essentially identical to that in Alport mice. These results strongly suggest that NR

protects the kidney *via* activating renal metabolism, more specifically, the RXR/PPARα signaling pathway that stimulates FAO. We then sought to confirm these results with orthogonal biochemical assays, but prior to doing so, we investigated potential sex differences in this mouse model of Alport syndrome.

Male and female Alport mice have distinct inflammatory and fibrotic responses

Alport syndrome affects both males and females, but it has not yet been reported if the disease progression differs between the sexes at the molecular level. Although several other studies have deposited RNA-seq datasets from Alport mouse kidneys to the Gene Expression Omnibus (48), all but three were from exclusively male mice (29, 30). Two studies did not specify the sex, but both reported data from three mice per group, implying that only a single sex was studied (49, 50). The sole study reporting RNA-seq data from both male and female Alport mice used a unique outbred model that is the first of its kind (51). No study thus far has investigated the kidney transcriptomic differences between male and female Alport mice using a common, commercially available genetic model. To address this gap, we analyzed the subset of 16 vehicle-treated mouse kidneys, four from each sex/genotype combination. This two-by-two factorial design allows for the robust identification of interactions between sex and genotype.

Principal component analysis showed that the data was tightly clustered with respect to both sex and genotype (**Fig. 5A**). PC1 accounted for 57.1% of the variance and was correlated with the genotype ($P = 4.66\times10^{-08}$). PC2 accounted for 14.3% of the variance and was correlated with sex ($P = 9.27\times10^{-08}$). Each of the remaining PCs accounted for less than 5% of the variance, and none were correlated with sex or genotype (data not shown).

A total of 114 genes were differentially regulated with both sex and disease, as identified by a sex:genotype interaction. This represents approximately three percent of the total 3842 genes that were statistically different between groups (**Fig. 5B**). GO enrichment analysis revealed that biological processes involved in the extracellular matrix and neovascularization were comparatively less upregulated in female Alport mice than in male Alport mice when compared to their sex-matched controls (**Figs. 5C**). In many cases, genes that were increased in female Alport mice (versus female control mice), such as the pro-fibrotic and pro-inflammatory genes *C3*, *Col1a2*, *Fgfbp1*, and *Ticam2* (**Fig. 5D**), were increased to a greater degree in male Alport mice (versus male control mice). We refer to this gene set as having a negative sex:genotype interaction because the increase in Alport mice compared to control mice is smaller (or even decreased, not increased) in female mice compared to male mice. An additional 70 genes had a negative sex:genotype interaction (**Fig. S21A**), while 40 genes had a positive sex:genotype interaction (**Fig. S21B**).

To further parse out the role of sex as a biological variable, pathway analysis using a modified GSEA algorithm was performed on the entire dataset as previously described (36, 52), not just the subset of genes with a significant sex:genotype interaction. This further identified inflammation-related pathways as differentially regulated with both sex and disease (**Fig. S22A-B**). This is best illustrated by visualization of the sex:genotype interaction data on a KEGG graph for the cytokine-cytokine receptor interaction pathway (**Fig. S22C**). There is a strong negative sex:genotype interaction across all of the plotted pro-inflammatory interactions. Also plotted on this KEGG graph is the TGF-β family which also displays a negative sex:genotype interaction, confirming the results of our previous analysis.

In summary, these data are robust evidence showing that fibrosis- and inflammation-related pathways are differentially regulated between the sexes in this mouse model of Alport syndrome. Importantly, neither analysis identified a sex:genotype interaction in metabolism-related pathways, our primary area of interest in this study. Therefore, we chose to only study male mice for all remaining biochemical assays because they seemed to have a more severe phenotype at the transcriptional level. However, the sexes were pooled for the snRNA-seq experiment due to the outsized benefit these data could have for the scientific community.

NAD^+ supplementation restores kidney mitochondrial fatty acid oxidation

Once we confirmed the absence of a sex:genotype interaction in metabolism-related pathways, we then returned to investigating the effects of NR treatment. Mitochondrial dysfunction is a well-accepted mechanism seen in models of CKD, including in a mouse model of Alport syndrome (29). In addition, enhancing *de novo* NAD^+ synthesis has been shown to improve mitochondrial FAO (53). Based on both our original hypothesis that decreased NAD^+ and subsequent metabolic dysregulation contribute to Alport disease, and our RNA-seq experiments that identified NR-mediated stimulation of fatty acid metabolic pathways, we hypothesized that mitochondrial FAO would be impaired in Alport mice and restored by NR treatment. To test this, we immunoblotted for key proteins in the mitochondrial FAO pathway: PGC-1α, carnitine palmitoyltransferase 1-α (CPT1α), and medium-chain acyl-coenzyme A dehydrogenase (MCAD).

PGC-1α is a coactivator that regulates PPARα function, and both CPT1α and MCAD are PPARα target genes (7, 54, 55). Consistent with the observed effects of NR in both control and

Alport mice on RNA-seq, PCG-1α levels were increased with NR treatment in both genotypes (**Fig. 6E-F**), and this serves as a good positive control for the effects of NR.

CPT1α and MCAD are both integral to mitochondrial FAO, and defects in either protein can cause severe clinical diseases (56). CPT1α controls fatty acyl-CoA transport into the mitochondria, and it is the rate-limiting step of long-chain FAO and medium-chain FAO of nine or more carbons in length (57). In our samples, CPT1α was reduced in Alport mice (versus control mice), and it was restored with NR treatment (**Figs. 6G** and **6I**). Medium-chain fatty acids, at least those up to eight carbons in length, can enter the mitochondria independent of CPT1α and then are converted to fatty acyl-CoAs once inside (57). However, regardless of how they enter the mitochondria, MCAD catalyzes the first step in mitochondrial FAO of all lengths of medium chain acyl-CoAs (56). In our samples, MCAD was also reduced in Alport mice (versus control mice) and restored by NR treatment (**Figs. 6I** and **6J**).

These changes in the key enzymes regulating both medium- and long-chain FAO are robust orthogonal data that validate the transcriptomic changes seen on RNA-seq. They further demonstrate that Alport mice have impaired fatty acid utilization and that NR protects the kidney by activating renal metabolism.

NAD^+ supplementation restores the canonical functions of the proximal tubule, and reduces immune cell and myofibroblast appearance, but it has minimal effect on the podocyte.

The data presented thus far strongly establish that NR protects the kidney via activating renal cortical transcription of metabolic genes, and this is associated with corresponding improvements in tubular mitochondrial morphology and renal expression of mitochondrial FAO proteins. However, they provide little insight into the molecular changes occurring within

individual cells. To investigate the cell type specific effects of NR treatment in Alport syndrome, as well as to show unambiguously that NR stimulates metabolism in the proximal tubules, we performed snRNA-seq on our samples.

Nuclei from control and Alport mice, both with and without NR treatment, were extracted, sequenced with snRNA-seq, and merged to create an atlas of thirty-one cell type clusters (**Fig. 7A**). Clusters were defined by known marker gene expression and most cell types were represented across all four conditions (**Fig. S23**). However, the proportion of cell type distribution varied across conditions (**Fig. 7B**). Podocytes and reference proximal tubule (PT) cells were more represented in control mice, whereas adaptive PT (aPT) and injured PT (iPT) had greater representation in Alport mice. Vehicle-treated Alport mice had enrichment of characteristic injury pathways in both the PT (**Fig. S24**) and podocytes (**Fig. S25**) as compared to vehicle-treated control mice. These pathways included fatty acid degradation, PPAR signaling, cell adhesion, and immune signaling. Osteopontin (*Spp1*) and Neutrophil gelatinase-associated lipocalin (*Lcn2*) were upregulated in both the PT and podocyte.

Although the injury phenotype of the Alport mice had many shared properties between the podocyte and proximal tubule cells, marked differential effects of NR treatment were observed between these two cell types. In the podocyte, NR treatment of Alport mice had minimal effect, with very few differentially expressed genes (**Fig. S26**). In contrast, the NR-treated proximal tubule had transcriptomic evidence supporting restoration of several of its vital cellular functions: translation (ribosome), metabolism, endocrine function, fatty acid degradation, and PPAR signaling (**Fig. 7C-D**). Spatial transcriptomic (ST) profiling confirmed the observed effects first seen in the snRNA-seq atlas (**Fig. 8**). ST revealed that expression of *Cpt1a*,

the rate limiting step for mitochondrial long-chain FAO, is reduced in Alport mice and restored with NR treatment. *Acadm* (the gene for MCAD) expression is reduced in the Alport condition and this reduction is mitigated with NR treatment. *Tfam* (mitochondrial transcription factor A) expression is similarly restored with NR treatment.

The proportions of myofibroblasts, macrophages, T lymphocytes and B lymphocytes were all increased in Alport mice within the snRNA-seq atlas. NR treatment was successful in reducing immune cell infiltration and fibrosis associated with the Alport condition. Using spatial transcriptomics, these cell types were localized to the tissue with a label transfer method (**Fig. S27**). NR treatment led to reduced immune cell infiltration and stromal cell appearance in Alport mice.

Taken together, these data suggest that NR treatment restores the canonical functions of the PT, reduces immune cell infiltration, and reduces myofibroblast appearance and fibrosis. Further, the effects of NR appear to be cell type specific with much greater effect observed in the PT than the podocyte.

Discussion

Herein, we have comprehensively shown that NR protects the kidney in a mouse model of Alport syndrome by activating renal metabolism in the proximal tubules. In addition, we report several other noteworthy contributions. We are the first to report sex-differences in the bulk renal transcriptome of Alport mice. We are also the first to report single cell (nuclei) transcriptome data of any kind from the Alport model, and we report data pooled from both male and female mice. Finally, at both the bulk and single cell (nuclei) level, we report that NR-mediated renal activation of metabolism occurs in healthy control mice and diseased Alport mice. The similarity in response between both control and Alport mice suggests that normalization of renal metabolism is the underlying nephroprotective mechanism of NAD^+ supplementation in CKD.

Using advance transcriptomic, biochemical, and imaging techniques we identified NR-mediated activation of the NAD^+–PGC-1α–PPARα–FAO axis as an important mechanism contributing to its nephroprotective effects. This is consistent with a substantial number of previous studies showing that activation of PPARα signaling protects the kidney, reviewed elsewhere (58). In fact, a prior study using Alport mice has already shown that activating mitochondrial metabolism via the PPARα pathway protects from kidney disease (29). Our study builds upon this research by identifying the importance of the NAD^+–PGC-1α axis, upstream to the PPARα–FAO axis. However, perhaps more importantly, we showed that the improvements in renal metabolism are the direct result of NAD^+ supplementation. They are not simply secondary to the prevention of kidney disease. The highly similar transcriptional responses of control and Alport mice to NAD^+ supplementation allows us to make this key mechanistic

insight, and it underscores the importance of also investigating the effects of drugs in the absence of disease.

Sex as a biological variable has been, and continues to be, a neglected area of research. It has been previously reported that male and female *Col4a3*^{tm1Dec} mice on the fast-progressing 129/SvJ background have similar severities of kidney disease (59). We note that this is unusual because male mice are generally more susceptible to kidney disease than female mice (60). Nevertheless, the current study used mice on the slow-progresing C57BL/6J background, and it was not designed as a comprehensive comparison between the sexes. Additional research is required, ideally a littermate-matched time course, to identify potential sex differences in clinically relevant markers of CKD. We speculate that the slow-progressing C57 background will be better suited for this than the fast-progressing 129 background because the former lives much longer than the latter.

However, our data do provide insight into the sex-differences in the bulk kidney cortical transcriptome in the Alport model. We identified 114 genes that have a sex:genotype interaction, confirming that kidney disease in this model of Alport syndrome manifests differently between the sexes, at least at the transcriptional level. Further analyses suggested that these genes modulate inflammation and fibrosis. This gene set represents a starting point that may assist in developing hypotheses to investigate the causative mechanism underlying a potential phenotypic sex-difference. It also suggests that Alport mice may have a sexually dimorphic response to some interventions that directly target inflammation- and fibrosis-related pathways, and researchers should take this into consideration when designing future studies.

Modern transcriptomic approaches, such as snRNA-seq, provide unparalleled insights into the molecular mechanisms of disease, and there is a focused effort to develop atlases with single-cell resolution (61). Because snRNA-seq is the still relatively new, datasets are not yet available for many disease models, especially rare diseases such as Alport syndrome. Our snRNA-seq dataset is the first of its kind from a model of Alport syndrome, and this makes it a noteworthy contribution in it of itself. In addition, we also report the first characterization of how NAD^+ supplementation affects the kidney at the single cell level in both states of health and disease. Our dataset is further differentiated by the inclusion of both sexes and the simultaneous assay for transposase-accessible chromatin, known as snATAC-seq. However, a full comparison between the sexes, as well as integration of the multiome data, is beyond the scope of the current publication.

Although it has been known that NAD^+ supplementation protects from CKD (10-14), the cell types which were responsible for this benefit were not rigorously investigated. Models of AKI displayed the strongest and most consistent therapeutic benefit of NAD^+ supplementation, implying the proximal tubules as a likely location. However, the data from models of CKD were less clear, and several studies suggested a potential role for podocytes. Podocytes from diabetic humans have reduced expression of genes in the *de novo* NAD^+ synthesis pathway, suggesting that podocyte NAD^+ levels might also be lower (62). Additionally, in a recent study using a model of diabetes, a fourteen-day course of nicotinamide mononucleotide at eight-weeks of age prevented diabetic CKD up to five months after stopping the intervention (12). This effect was attributed to sirtuin 1-mediated epigenetic regulation within the podocytes, although podocyte-specific *Sirt1*-null mice were not used. Our data clearly shows, with single-cell

resolution, that the effects of NAD^+ supplementation are many orders of magnitude greater in the proximal tubules than in the podocytes. This difference is so large that, at least on the transcriptional level, the effect of NAD^+ supplementation on podocytes is likely negligible in this mouse model of Alport syndrome.

This raises several interesting questions, including how NAD^+ supplementation can successfully decrease albuminuria and restore other markers of glomerular disease if it does not directly modulate podocytes. This tubular-glomerular interaction in CKD is usually discussed the other way around; namely, that tubular disease in proteinuric CKD models is the sole result of glomerular disease. We make no claims to the contrary here. However, we do not believe that this implies that all interventions that improve glomerular function must directly target the glomerulus. In fact, there is emergent research that indicates glomerular disease can be indirectly modified by tubular processes. Specific injury to the proximal tubules can cause proteinuria and glomerulosclerosis (63). Conversely, protective tubular processes can also protect the glomerulus (64). In this context, it seems likely that the reduction in glomerular markers of CKD we observed in the current study were secondary to the protective effects of NR in the tubules.

In summary, NAD^+ supplementation protects the kidney in a mouse model of Alport syndrome. Mechanistically, NR activates renal metabolism by restoring the NAD^+–PGC-1α–PPARα–FAO axis within the proximal tubules. Furthermore, NAD^+ supplementation with NR has essentially no direct effects on the podocytes, implying that observed improvements in glomerular pathology are the result of the prevention of tubular damage. This important

mechanistic insight should cause researchers to consider repurposing other tubular drugs for the treatment of primary glomerular diseases.

Acknowledgments

We acknowledge all Levi Lab members, as well as our collaborators, for their thought-provoking questions. We thank Bo Zhang and Amanda Knoten for assistance with the snRNA-seq experiments and the Washington University Kidney Translational Research Center for support. Research reported in this publication was supported by the National Institutes of Health Grants National Institutes of Health Grants F30DK129003 (to B.A.J.), R01DK116567 (to M.L.), R01DK127830 (to M.L.), TL1TR001431 (to B.A.J.), P30CA051008, and the Washington University Pediatric Center of Excellence in Nephrology grant P50DK133943 (S.J. and M.T.E).

Conflict-of-interest statement

The authors have nothing to disclose.

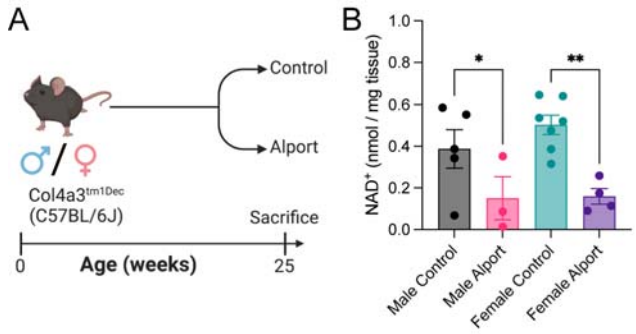

Figure 1: Kidney NAD$^+$ is reduced in Alport mice. (**A**) Experimental design: Control and Alport mice of both sexes were sacrificed at 25-weeks of age. (**B**) Alport mice had lower levels of kidney NAD$^+$ than control mice. Significance was determined by one-way ANOVA with the Holm–Šídák correction for multiple comparisons. Data are expressed as the means ± SEM, and each datum represents one mouse.

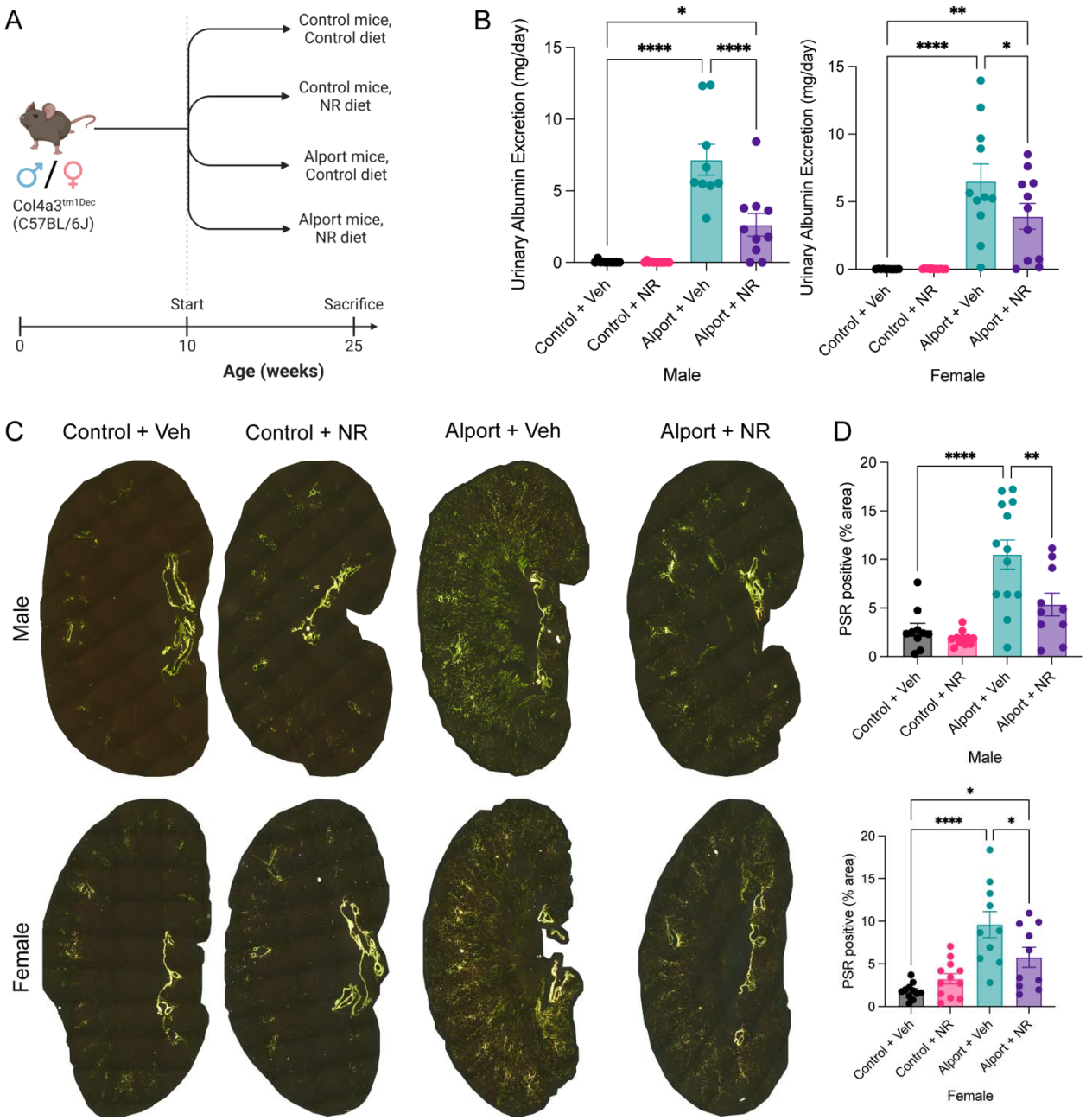

Figure 2: NAD$^+$ supplementation protects the kidney in Alport mice. (**A**) Experimental design: Control and Alport mice of both sexes were treated with or without NR between 10-weeks and 25-weeks of age. (**B**) NR treatment reduced 24-hour urinary albumin excretion in Alport mice of both sexes. (**C**) Representative images of PSR-stained kidneys acquired with polarized light. Yellow-green-orange birefringence is highly specific for fibrosis. (**D**) Quantification of PSR-

stained kidneys shows that NR treatment reduced renal fibrosis in both sexes. Significance was determined by one-way ANOVA with the Holm–Šídák correction for multiple comparisons. Data are expressed as the means ± SEM, and each datum represents one mouse. *$P < 0.05$, **$P < 0.01$, ****$P < 0.0001$. NR, nicotinamide riboside; PSR, picrosirius red; Veh, vehicle.

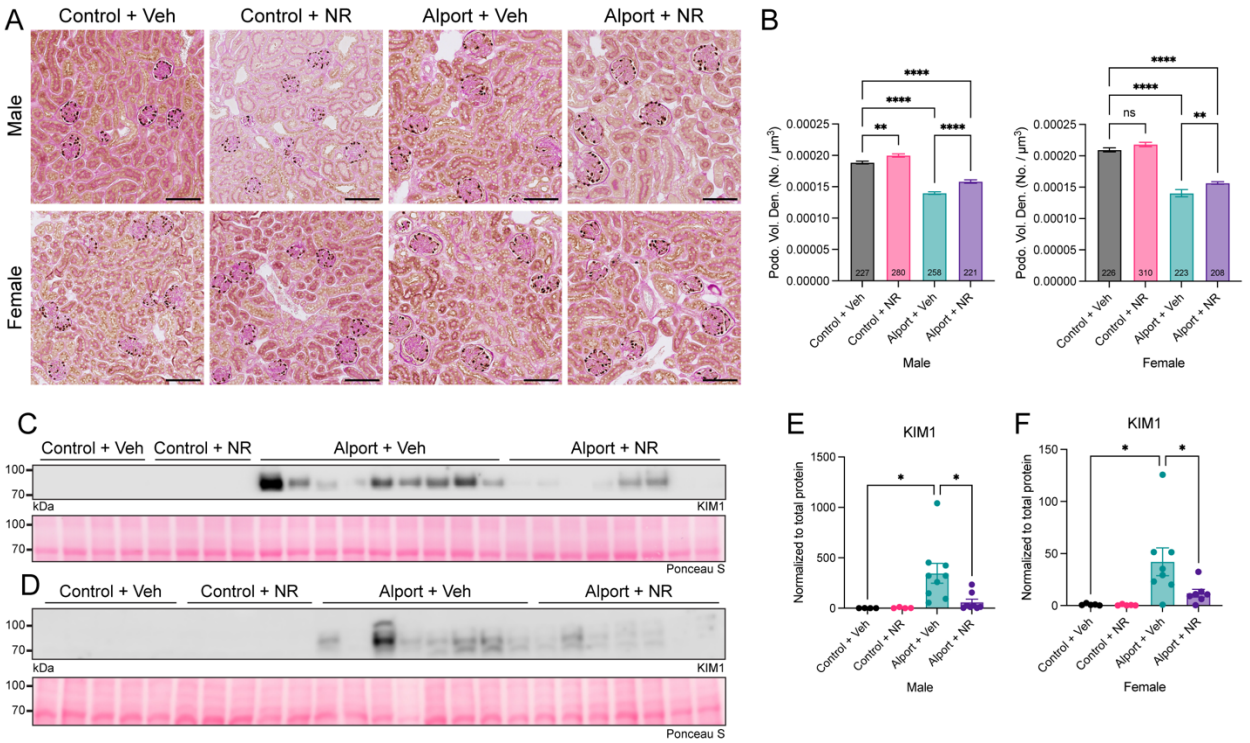

Figure 3: NAD$^+$ supplementation prevents both glomerular and tubular injury in Alport mice. (**A**) Representative images of immunohistochemistry for p57^{kip2}, followed by periodic acid–Schiff post-staining without hematoxylin counterstaining. Podocyte nuclei are stained brown, and all other glomerular structures are stained pink. (**B**) Quantification of p57^{kip2} immunostaining with PodoCount, a validated algorithm to analyze p57^{kip2}-stained whole slide images. Podocyte volumetric density was reduced in Alport mice and restored by NR treatment in both sexes. (**C,D**) Immunoblots for KIM-1, a tubular injury marker, in male (*C*) and female (*D*) kidney homogenate. Ponceau S, a nonspecific protein stain, was used as a loading control. (**E,F**) Quantification of immunoblots (*C,D*) shows that KIM-1 is increased in Alport mice and reduced by NR treatment in male (*E*) and female (*F*) mice. Scale bars represent 100 µm. Significance was determined by one-way ANOVA with the Holm–Šídák correction for multiple comparisons. Data are expressed as the means ± SEM. Each datum represents one glomeruli (*B*) or one mouse (*E*-

F). *$P < 0.05$, **$P < 0.01$, ****$P < 0.0001$. Kidney injury molecule-1, KIM-1; NR, nicotinamide riboside; PSR, picrosirius red; Veh, vehicle.

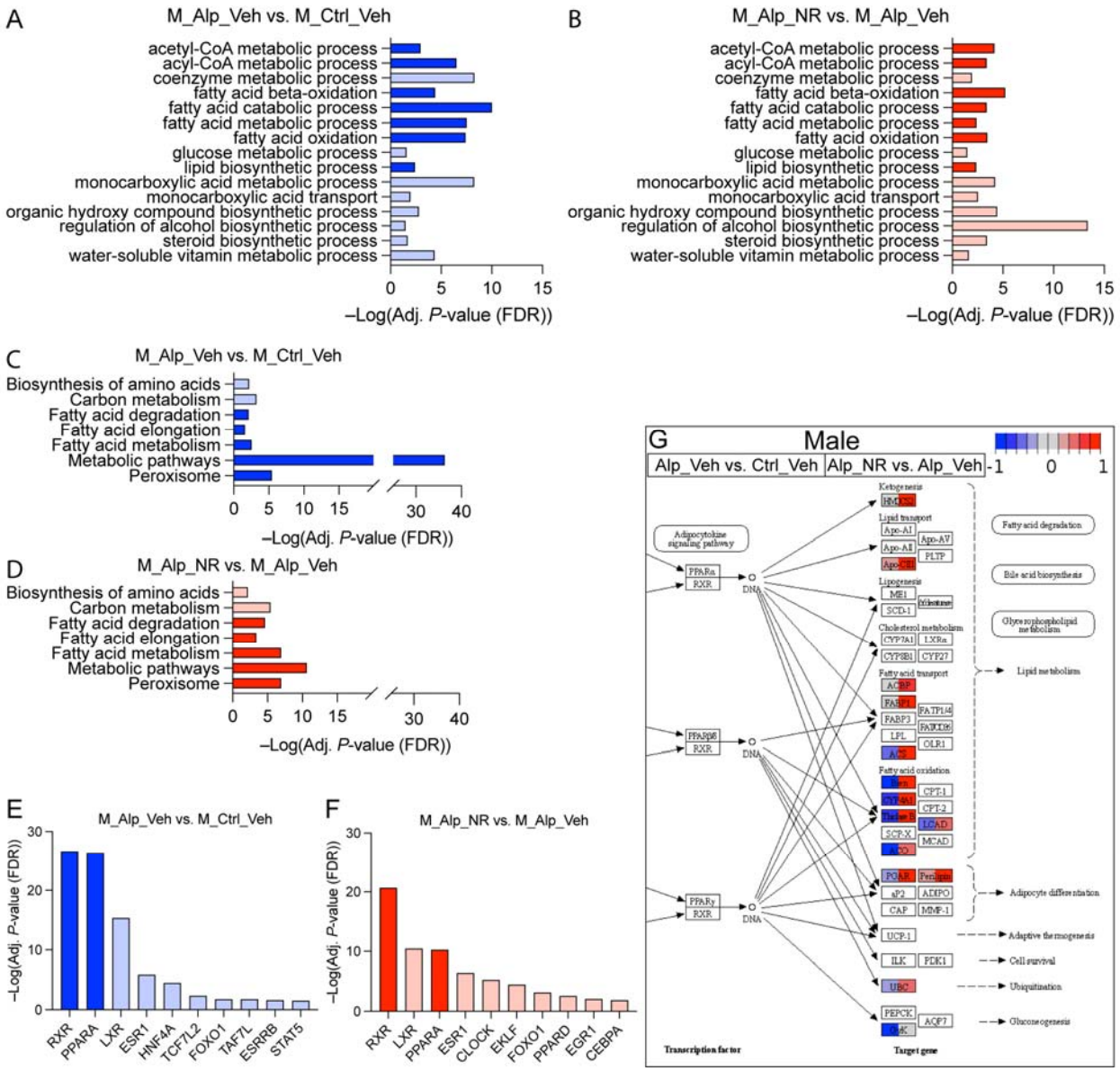

Figure 4: NAD$^+$ supplementation activates renal metabolism in male mice. Bulk kidney cortex RNA-seq data from male control and Alport mice, treated with or without NR, were analyzed. (**A,B**) Gene ontology (GO) biological processes that are both (*A*) reduced in vehicle-treated Alport mice (vs. vehicle-treated control mice) and (*B*) increased in NR-treated Alport mice (vs. vehicle-treated Alport mice) are shown. (**C,D**) KEGG pathways that are both (*C*) reduced in vehicle-treated Alport mice (vs. vehicle-treated control mice) and (*D*) increased in NR-treated Alport mice (vs. vehicle-treated Alport mice) are shown. (**E,F**) Transcription factor analyses

suggest that the RXR/PPARα gene regulatory network is (*E*) inhibited in vehicle-treated Alport mice (vs. vehicle-treated control mice) and (*F*) activated in NR-treated Alport mice (vs. vehicle-treated Alport mice). Processes (*A*,*B*), pathways (*C*,*D*), and transcription factors (*E*,*F*) that are directly involved in fatty acid metabolism are highly enriched in all comparisons, emphasized by either dark blue (decreased) or dark red (increased). (**G**) Partial KEGG graph for the PPAR signaling pathway (KEGG Entry No. 03320). The left and right sides of each gene box represent data from vehicle-treated male Alport mice (vs. vehicle-treated male control mice) and NR-treated male Alport mice (vs. vehicle-treated male Alport mice), respectively. The sub-pathway that was the most restored by NR treatment was fatty acid oxidation. Alp, Alport; Ctrl, control; M, male; NR, nicotinamide riboside; Veh, vehicle.

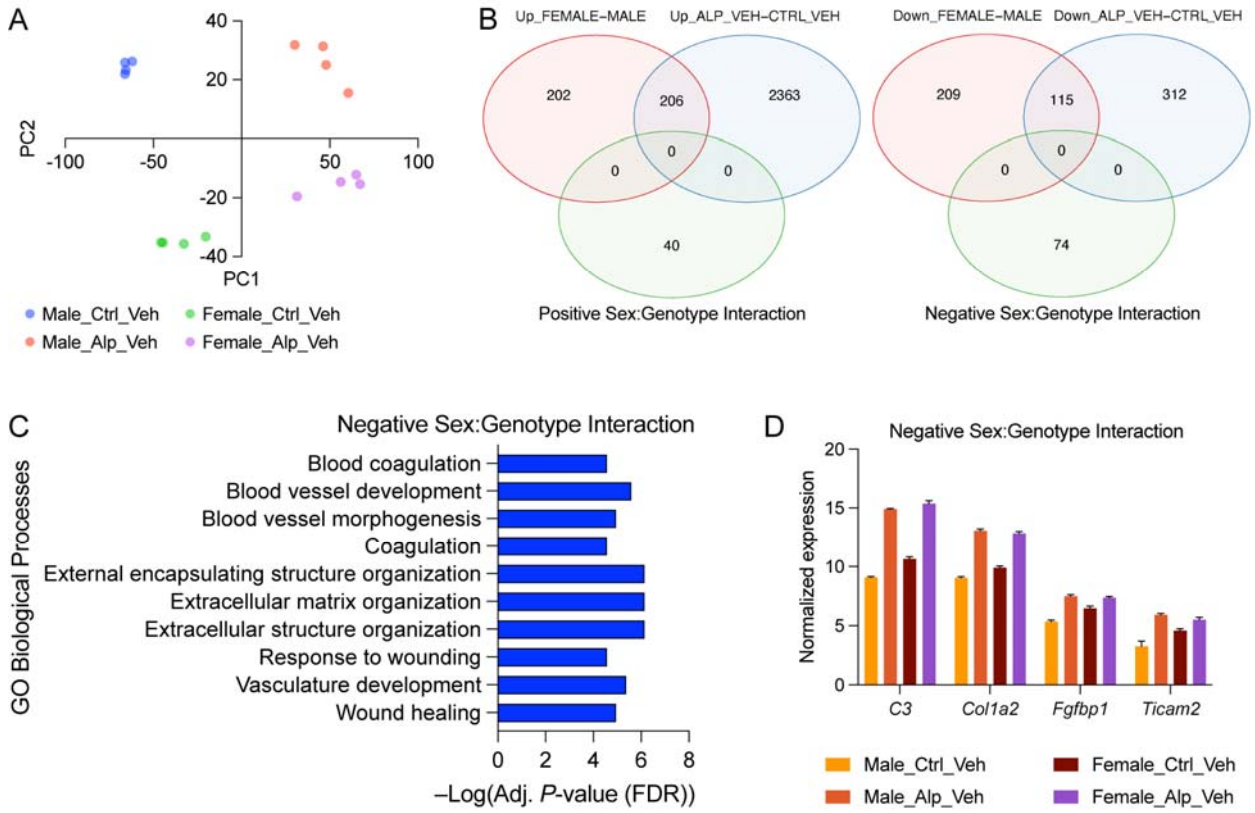

Figure 5: The *Col4a3*^{tm1Dec} mouse model of Alport syndrome has sex differences at the transcriptional level. (**A**) Principal component analysis shows good separation between samples by both genotype (PC1) and sex (PC2). (**B**) Venn diagrams showing the number of genes that are differentially regulated between the sexes (*red*) or genotypes (*blue*). Genes with a sex:genotype interaction are shown in green. A positive interaction (*left diagram, green*) indicates that, when comparing genotypes of the same sex, these genes are upregulated (or less downregulated) in the female genotype comparison versus the male genotype comparison. A negative interaction (*right diagram, green*) indicates the reverse of this. (**C**) Gene ontology (GO) biological processes related to fibrosis and neovascularization displayed a significant negative sex:genotype interaction. All statistically significant changes are plotted, and no GO biological processes had a positive sex:genotype interaction. (**D**) Examples of genes related to

inflammation (*C3* and *Ticam2*) and fibrosis (*Col1a2* and *Fgfbp1*) that have a negative sex:genotype interaction. This means that, when comparing genotypes of the same sex, these genes are downregulated (or, as in these four cases, less upregulated) in the female genotype comparison versus the male genotype comparison. Each group is composed of data from four biological replicates.

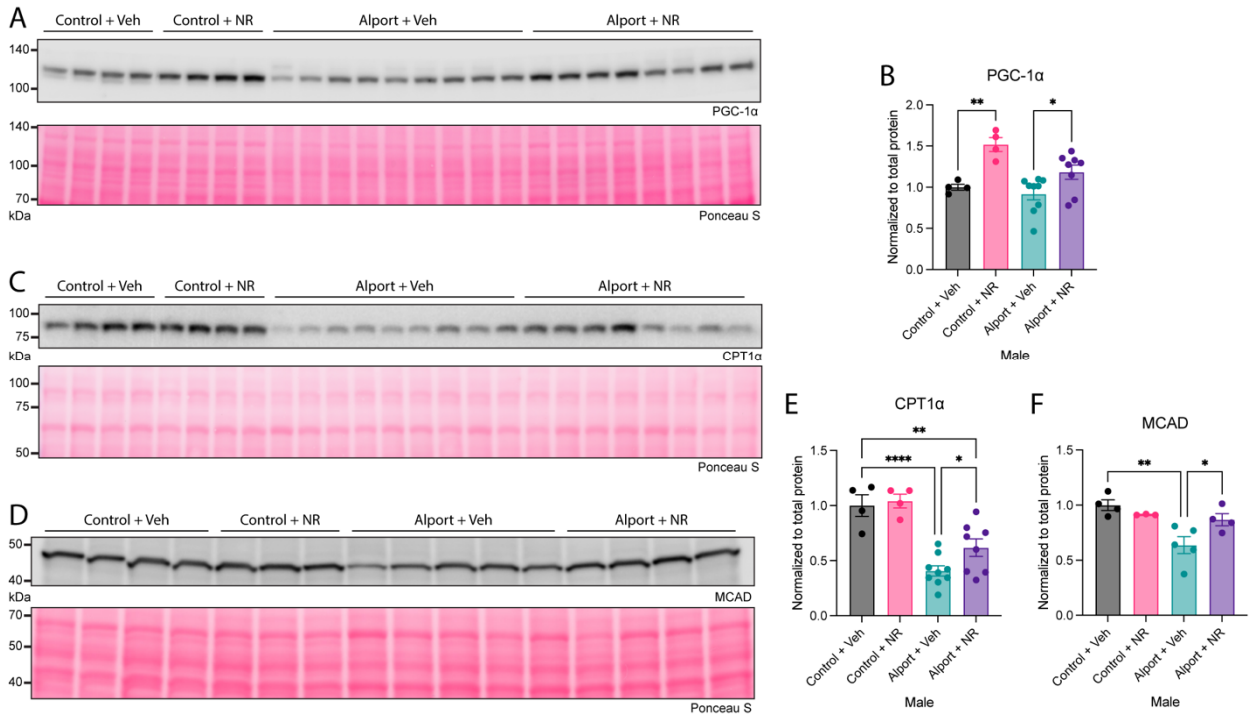

Figure 6: NAD$^+$ supplementation restores tubular mitochondrial morphology and activates renal fatty acid metabolism. (**A,B**) NR treatment increased kidney PGC-1α in both control and Alport mice. (**C-F**) Kidney CPT1α (*C,E*) and MCAD (*D,F*), key players in mitochondrial fatty acid oxidation, were reduced in Alport mice and restored by NR treatment. Ponceau S, a nonspecific protein stain, was used as a loading control. Significance was determined by one-way ANOVA with the Holm–Šídák correction for multiple comparisons. Data are expressed as the means ± SEM. Each datum represents one mouse. *$P < 0.05$, **$P < 0.01$, ****$P < 0.0001$. CPT1α, carnitine palmitoyltransferase 1-α; MCAD, medium-chain acyl-coenzyme A dehydrogenase; NR, nicotinamide riboside; PGC-1α, peroxisome proliferator-activated receptor-γ coactivator 1-α; Veh, vehicle.

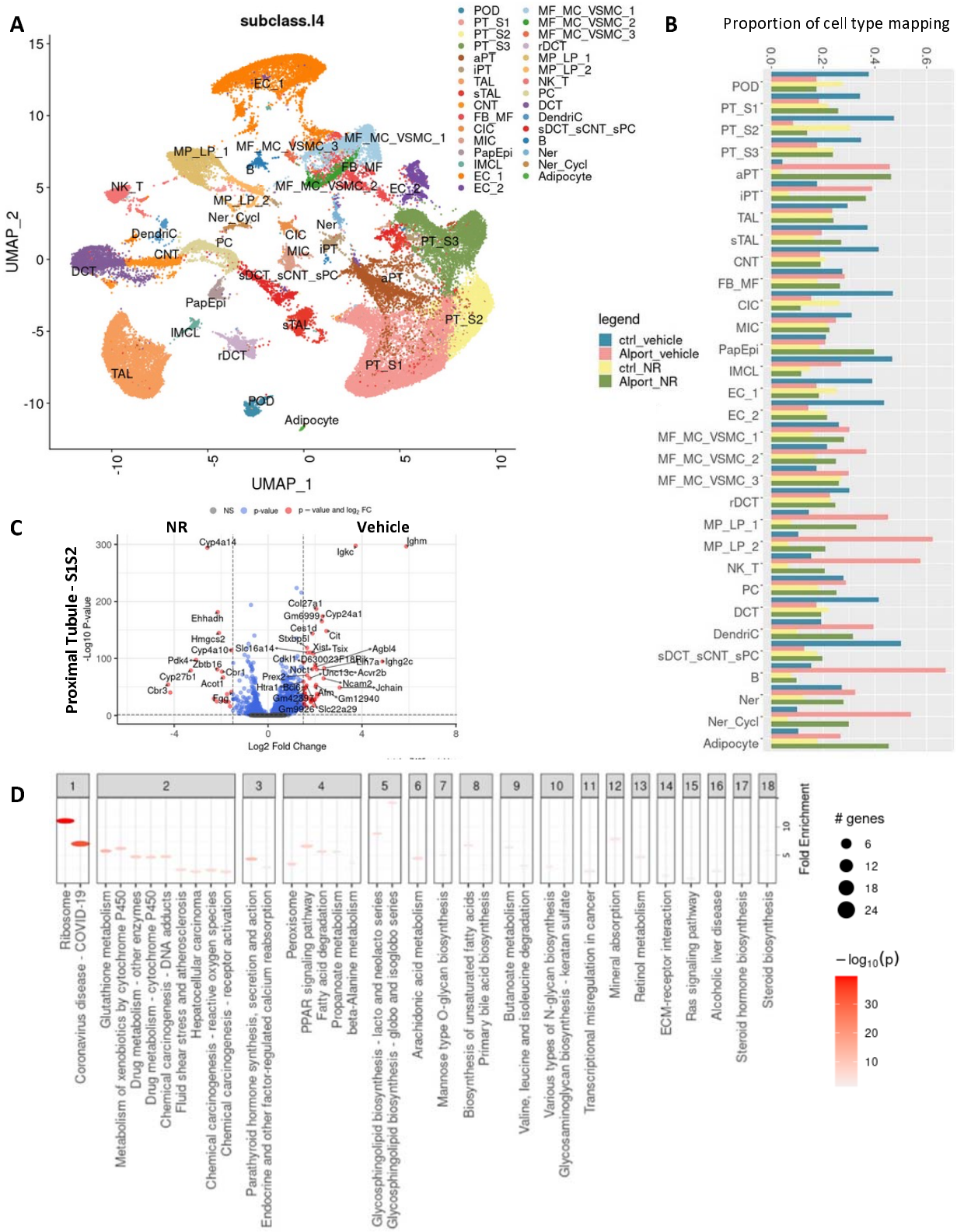

Figure 7: Single nucleus RNA-sequencing of control and Alport mice, with and without NAD$^+$ supplementation. (**A**) The snRNA-seq reduction by uniform manifold approximation and

projection (UMAP) of 49,488 nuclei in 31 clusters. (**B**) Proportion of nuclei per cluster by condition. Myofibroblasts and immune cells were upregulated in Alport mice. The effect was mitigated by NR treatment. (**C**) Differentially expressed genes in Alport mice treated with NR or vehicle (genes upregulated in vehicle are displayed on the right). Mice treated with NR had reduced expression of immune signaling transcripts such as *Ncam2* and *Jchain*. (**D**) Enriched pathways between Alport mice treated with vehicle and NR. NR treatment significantly impacted translation (ribosome), metabolism, endocrine function, and PPAR signaling in the proximal tubule cell.

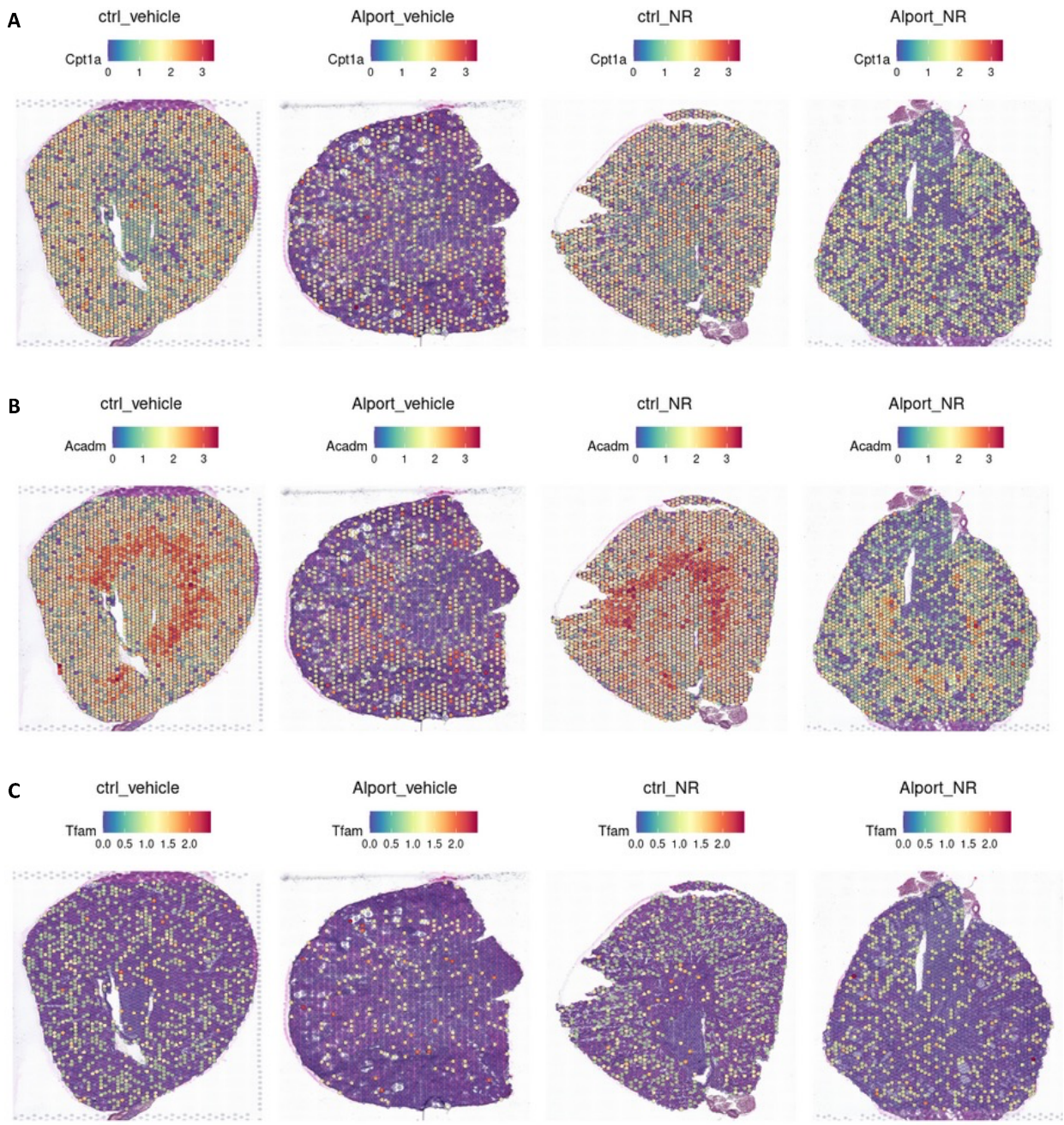

Figure 8: Spatial localization of gene expression across 8,748 spots. Visium spatial transcriptomics was performed on vehicle-treated male control mice (*far left*), vehicle-treated male Alport mice (*center left*), NR-treated male control mice (*center right*), and NR-treated male Alport mice (*far right*). (**A-C**) *Cpt1a* (*A*), *Adcam* (*B*), and *Tfam* (*C*) expression are reduced in Alport mice and restored with NR treatment.

References

1. Romagnani P, Remuzzi G, Glassock R, Levin A, Jager KJ, Tonelli M, et al. Chronic kidney disease. *Nat Rev Dis Primers.* 2017;3:17088.
2. Katsyuba E, Romani M, Hofer D, and Auwerx J. NAD(+) homeostasis in health and disease. *Nat Metab.* 2020;2(1):9-31.
3. Ralto KM, Rhee EP, and Parikh SM. NAD(+) homeostasis in renal health and disease. *Nat Rev Nephrol.* 2020;16(2):99-111.
4. Poyan Mehr A, Tran MT, Ralto KM, Leaf DE, Washco V, Messmer J, et al. De novo NAD(+) biosynthetic impairment in acute kidney injury in humans. *Nat Med.* 2018;24(9):1351-9.
5. Morevati M, Fang EF, Mace ML, Kanbay M, Gravesen E, Nordholm A, et al. Roles of NAD(+) in Acute and Chronic Kidney Diseases. *Int J Mol Sci.* 2022;24(1).
6. Tran MT, Zsengeller ZK, Berg AH, Khankin EV, Bhasin MK, Kim W, et al. PGC1alpha drives NAD biosynthesis linking oxidative metabolism to renal protection. *Nature.* 2016;531(7595):528-32.
7. Vega RB, Huss JM, and Kelly DP. The coactivator PGC-1 cooperates with peroxisome proliferator-activated receptor alpha in transcriptional control of nuclear genes encoding mitochondrial fatty acid oxidation enzymes. *Mol Cell Biol.* 2000;20(5):1868-76.
8. Liu X, Luo D, Huang S, Liu S, Zhang B, Wang F, et al. Impaired Nicotinamide Adenine Dinucleotide Biosynthesis in the Kidney of Chronic Kidney Disease. *Front Physiol.* 2021;12:723690.
9. Faivre A, Katsyuba E, Verissimo T, Lindenmeyer M, Rajaram RD, Naesens M, et al. Differential role of nicotinamide adenine dinucleotide deficiency in acute and chronic kidney disease. *Nephrol Dial Transplant.* 2021;36(1):60-8.
10. Zheng M, Cai J, Liu Z, Shu S, Wang Y, Tang C, et al. Nicotinamide reduces renal interstitial fibrosis by suppressing tubular injury and inflammation. *J Cell Mol Med.* 2019;23(6):3995-4004.
11. Kumakura S, Sato E, Sekimoto A, Hashizume Y, Yamakage S, Miyazaki M, et al. Nicotinamide Attenuates the Progression of Renal Failure in a Mouse Model of Adenine-Induced Chronic Kidney Disease. *Toxins (Basel).* 2021;13(1).
12. Yasuda I, Hasegawa K, Sakamaki Y, Muraoka H, Kawaguchi T, Kusahana E, et al. Pre-emptive Short-term Nicotinamide Mononucleotide Treatment in a Mouse Model of Diabetic Nephropathy. *J Am Soc Nephrol.* 2021;32(6):1355-70.
13. Zhen X, Zhang S, Xie F, Zhou M, Hu Z, Zhu F, et al. Nicotinamide Supplementation Attenuates Renal Interstitial Fibrosis via Boosting the Activity of Sirtuins. *Kidney Dis (Basel).* 2021;7(3):186-99.
14. Myakala K, Wang XX, Shults NV, Krawczyk E, Jones BA, Yang X, et al. NAD metabolism modulates inflammation and mitochondria function in diabetic kidney disease. *J Biol Chem.* 2023;299(8):104975.
15. Takahashi R, Kanda T, Komatsu M, Itoh T, Minakuchi H, Urai H, et al. The significance of NAD + metabolites and nicotinamide N-methyltransferase in chronic kidney disease. *Sci Rep.* 2022;12(1):6398.
16. Wei PZ, and Szeto CC. Mitochondrial dysfunction in diabetic kidney disease. *Clin Chim Acta.* 2019;496:108-16.

17. Doke T, and Susztak K. The multifaceted role of kidney tubule mitochondrial dysfunction in kidney disease development. *Trends Cell Biol.* 2022;32(10):841-53.
18. Miguel V, Tituana J, Herrero JI, Herrero L, Serra D, Cuevas P, et al. Renal tubule Cpt1a overexpression protects from kidney fibrosis by restoring mitochondrial homeostasis. *J Clin Invest.* 2021;131(5).
19. Brinkkoetter PT, Bork T, Salou S, Liang W, Mizi A, Ozel C, et al. Anaerobic Glycolysis Maintains the Glomerular Filtration Barrier Independent of Mitochondrial Metabolism and Dynamics. *Cell Rep.* 2019;27(5):1551-66 e5.
20. Guo J, Song W, Boulanger J, Xu EY, Wang F, Zhang Y, et al. Dysregulated Expression of microRNA-21 and Disease-Related Genes in Human Patients and in a Mouse Model of Alport Syndrome. *Hum Gene Ther.* 2019;30(7):865-81.
21. Cosgrove D, Meehan DT, Grunkemeyer JA, Kornak JM, Sayers R, Hunter WJ, et al. Collagen COL4A3 knockout: a mouse model for autosomal Alport syndrome. *Genes Dev.* 1996;10(23):2981-92.
22. Dall M, Trammell SAJ, Asping M, Hassing AS, Agerholm M, Vienberg SG, et al. Mitochondrial function in liver cells is resistant to perturbations in NAD(+) salvage capacity. *J Biol Chem.* 2019;294(36):13304-26.
23. Pistner A, Belmonte S, Coulthard T, and Blaxall B. Murine echocardiography and ultrasound imaging. *J Vis Exp.* 2010(42).
24. Lindsey ML, Kassiri Z, Virag JAI, de Castro Bras LE, and Scherrer-Crosbie M. Guidelines for measuring cardiac physiology in mice. *Am J Physiol Heart Circ Physiol.* 2018;314(4):H733-H52.
25. Jones BA, Myakala K, Guha M, Davidson S, Adapa S, Lopez Santiago I, et al. Farnesoid X receptor prevents neutrophil extracellular traps via reduced sphingosine-1-phosphate in chronic kidney disease. *Am J Physiol Renal Physiol.* 2023;325(6):F792-F810.
26. Schindelin J, Arganda-Carreras I, Frise E, Kaynig V, Longair M, Pietzsch T, et al. Fiji: an open-source platform for biological-image analysis. *Nat Methods.* 2012;9(7):676-82.
27. Santo BA, Govind D, Daneshpajouhnejad P, Yang X, Wang XX, Myakala K, et al. PodoCount: A Robust, Fully Automated, Whole-Slide Podocyte Quantification Tool. *Kidney Int Rep.* 2022;7(6):1377-92.
28. Shumway M, Cochrane G, and Sugawara H. Archiving next generation sequencing data. *Nucleic Acids Res.* 2010;38(Database issue):D870-1.
29. Gomez IG, MacKenna DA, Johnson BG, Kaimal V, Roach AM, Ren S, et al. Anti-microRNA-21 oligonucleotides prevent Alport nephropathy progression by stimulating metabolic pathways. *J Clin Invest.* 2015;125(1):141-56.
30. Rubel D, Boulanger J, Craciun F, Xu EY, Zhang Y, Phillips L, et al. Anti-microRNA-21 Therapy on Top of ACE Inhibition Delays Renal Failure in Alport Syndrome Mouse Models. *Cells.* 2022;11(4).
31. Torre D, Lachmann A, and Ma'ayan A. BioJupies: Automated Generation of Interactive Notebooks for RNA-Seq Data Analysis in the Cloud. *Cell Syst.* 2018;7(5):556-61 e3.
32. Ashburner M, Ball CA, Blake JA, Botstein D, Butler H, Cherry JM, et al. Gene ontology: tool for the unification of biology. The Gene Ontology Consortium. *Nat Genet.* 2000;25(1):25-9.

33. Gene Ontology C, Aleksander SA, Balhoff J, Carbon S, Cherry JM, Drabkin HJ, et al. The Gene Ontology knowledgebase in 2023. *Genetics.* 2023;224(1).
34. Kanehisa M, and Goto S. KEGG: kyoto encyclopedia of genes and genomes. *Nucleic Acids Res.* 2000;28(1):27-30.
35. Kanehisa M, Furumichi M, Sato Y, Kawashima M, and Ishiguro-Watanabe M. KEGG for taxonomy-based analysis of pathways and genomes. *Nucleic Acids Res.* 2023;51(D1):D587-D92.
36. Ge SX, Son EW, and Yao R. iDEP: an integrated web application for differential expression and pathway analysis of RNA-Seq data. *BMC Bioinformatics.* 2018;19(1):534.
37. Luo W, Pant G, Bhavnasi YK, Blanchard SG, Jr., and Brouwer C. Pathview Web: user friendly pathway visualization and data integration. *Nucleic Acids Res.* 2017;45(W1):W501-W8.
38. Luo W, and Brouwer C. Pathview: an R/Bioconductor package for pathway-based data integration and visualization. *Bioinformatics.* 2013;29(14):1830-1.
39. Gisch DL, Brennan M, Lake BB, Basta J, Keller MS, Melo Ferreira R, et al. The chromatin landscape of healthy and injured cell types in the human kidney. *Nat Commun.* 2024;15(1):433.
40. Lake BB, Menon R, Winfree S, Hu Q, Melo Ferreira R, Kalhor K, et al. An atlas of healthy and injured cell states and niches in the human kidney. *Nature.* 2023;619(7970):585-94.
41. Ulgen E, Ozisik O, and Sezerman OU. pathfindR: An R Package for Comprehensive Identification of Enriched Pathways in Omics Data Through Active Subnetworks. *Front Genet.* 2019;10:858.
42. Melo Ferreira R, Sabo AR, Winfree S, Collins KS, Janosevic D, Gulbronson CJ, et al. Integration of spatial and single-cell transcriptomics localizes epithelial cell-immune cross-talk in kidney injury. *JCI Insight.* 2021;6(12).
43. Junqueira LC, Bignolas G, and Brentani RR. Picrosirius staining plus polarization microscopy, a specific method for collagen detection in tissue sections. *Histochem J.* 1979;11(4):447-55.
44. Satirapoj B, Nast CC, and Adler SG. Novel insights into the relationship between glomerular pathology and progressive kidney disease. *Adv Chronic Kidney Dis.* 2012;19(2):93-100.
45. Nangaku M. Mechanisms of tubulointerstitial injury in the kidney: final common pathways to end-stage renal failure. *Intern Med.* 2004;43(1):9-17.
46. Ichimura T, Bonventre JV, Bailly V, Wei H, Hession CA, Cate RL, et al. Kidney injury molecule-1 (KIM-1), a putative epithelial cell adhesion molecule containing a novel immunoglobulin domain, is up-regulated in renal cells after injury. *J Biol Chem.* 1998;273(7):4135-42.
47. Ichimura T, Hung CC, Yang SA, Stevens JL, and Bonventre JV. Kidney injury molecule-1: a tissue and urinary biomarker for nephrotoxicant-induced renal injury. *Am J Physiol Renal Physiol.* 2004;286(3):F552-63.
48. Barrett T, Wilhite SE, Ledoux P, Evangelista C, Kim IF, Tomashevsky M, et al. NCBI GEO: archive for functional genomics data sets--update. *Nucleic Acids Res.* 2013;41(Database issue):D991-5.

49. Zhu Z, Rosenkranz KAT, Kusunoki Y, Li C, Klaus M, Gross O, et al. Finerenone Added to RAS/SGLT2 Blockade for CKD in Alport Syndrome. Results of a Randomized Controlled Trial with Col4a3-/- Mice. *J Am Soc Nephrol.* 2023;34(9):1513-20.
50. Soloyan H, Thornton M, Villani V, Khatchadourian P, Cravedi P, Angeletti A, et al. Glomerular endothelial cell heterogeneity in Alport syndrome. *Sci Rep.* 2020;10(1):11414.
51. Takemon Y, Wright V, Davenport B, Gatti DM, Sheehan SM, Letson K, et al. Uncovering Modifier Genes of X-Linked Alport Syndrome Using a Novel Multiparent Mouse Model. *J Am Soc Nephrol.* 2021;32(8):1961-73.
52. Korotkevich G, Sukhov V, Budin N, Shpak B, Artyomov MN, and Sergushichev A. Fast gene set enrichment analysis. *bioRxiv.* 2021:060012.
53. Katsyuba E, Mottis A, Zietak M, De Franco F, van der Velpen V, Gariani K, et al. De novo NAD(+) synthesis enhances mitochondrial function and improves health. *Nature.* 2018;563(7731):354-9.
54. Gulick T, Cresci S, Caira T, Moore DD, and Kelly DP. The peroxisome proliferator-activated receptor regulates mitochondrial fatty acid oxidative enzyme gene expression. *Proc Natl Acad Sci U S A.* 1994;91(23):11012-6.
55. Napal L, Marrero PF, and Haro D. An intronic peroxisome proliferator-activated receptor-binding sequence mediates fatty acid induction of the human carnitine palmitoyltransferase 1A. *J Mol Biol.* 2005;354(4):751-9.
56. Houten SM, Violante S, Ventura FV, and Wanders RJ. The Biochemistry and Physiology of Mitochondrial Fatty Acid beta-Oxidation and Its Genetic Disorders. *Annu Rev Physiol.* 2016;78:23-44.
57. Schonfeld P, and Wojtczak L. Short- and medium-chain fatty acids in energy metabolism: the cellular perspective. *J Lipid Res.* 2016;57(6):943-54.
58. Jones BA, Wang XX, Myakala K, and Levi M. Nuclear Receptors and Transcription Factors in Obesity-Related Kidney Disease. *Semin Nephrol.* 2021;41(4):318-30.
59. Kim M, Piaia A, Shenoy N, Kagan D, Gapp B, Kueng B, et al. Progression of Alport Kidney Disease in Col4a3 Knock Out Mice Is Independent of Sex or Macrophage Depletion by Clodronate Treatment. *PLoS One.* 2015;10(11):e0141231.
60. Bairey Merz CN, Dember LM, Ingelfinger JR, Vinson A, Neugarten J, Sandberg KL, et al. Sex and the kidneys: current understanding and research opportunities. *Nat Rev Nephrol.* 2019;15(12):776-83.
61. Hu BC. The human body at cellular resolution: the NIH Human Biomolecular Atlas Program. *Nature.* 2019;574(7777):187-92.
62. Zhang Y, Zhao X, Li C, Yang Y, Li L, Chen Y, et al. Aberrant NAD synthetic flux in podocytes under diabetic conditions and effects of indoleamine 2,3-dioxygenase on promoting de novo NAD synthesis. *Biochem Biophys Res Commun.* 2023;643:61-8.
63. Grgic I, Campanholle G, Bijol V, Wang C, Sabbisetti VS, Ichimura T, et al. Targeted proximal tubule injury triggers interstitial fibrosis and glomerulosclerosis. *Kidney Int.* 2012;82(2):172-83.
64. Tan RJ, Li Y, Rush BM, Cerqueira DM, Zhou D, Fu H, et al. Tubular injury triggers podocyte dysfunction by beta-catenin-driven release of MMP-7. *JCI Insight.* 2019;4(24).